HOWARD UNIVERSITY

Notes on ADSORPTION

by Silvina Gatica and Hind Aljaddani

Chapter 1

Introduction

According to the Environmental Protection Agency (EPA), hazardous air pollutants are the cause of serious health and environmental problems [1]. CO_2, CH_4 and NO_2 are major harmful molecules whose concentration in the atmosphere increases dramatically as a result of burning of fossil fuels, transportation and industrial emissions, power plants and human activities [2]. Separating CO_2 from CH_4 is critical in industrial applications, transportation and usage of methane, especially in the prevention of equipment and pipelines corrosion [3].

Researchers have intensively investigated several materials, like MOFs, mesoporous carbon, activated carbon, silicalite, C_{186} schwarzite and nanoporous carbon, experimentally and theoretically, to capture, separate and store gases [3–11]. Based on previous studies of adsorption of CO_2 mixtures at room temperature, the selectivity still needs to be improved to achieve efficient separation.

1.1 Physical Adsorption

Physical adsorption (physisorption) is a term applied to atoms or molecules that are weakly bound to surfaces. In physical adsorption, van der Waals forces are dominant and no chemical bonds are formed. Physical adsorption is a reversible process so the substrate can be used repeatedly. The specification of an appropriate adsorbent is the key for separation by adsorption. Carbon-based materials have been considered promising substrates for gas sorption, storage, and separation, because of their abundance, robust pore structure, tunable porosity, specific area, light-weight, hight thermal and chemical stability, low cost, and easy scale-up associated with their manufacturing [13].

Physical adsorption occurs when the vapor (the absorptive) is in equilibrium with a substrate (adsorbent); atoms stick to the substrate to form a film (adsorbate) as shown in Figure 1.1. Heat is an important factor in physical adsorption: at low temperature, adsorption is high whereas at high-temperature atoms desorb [14].

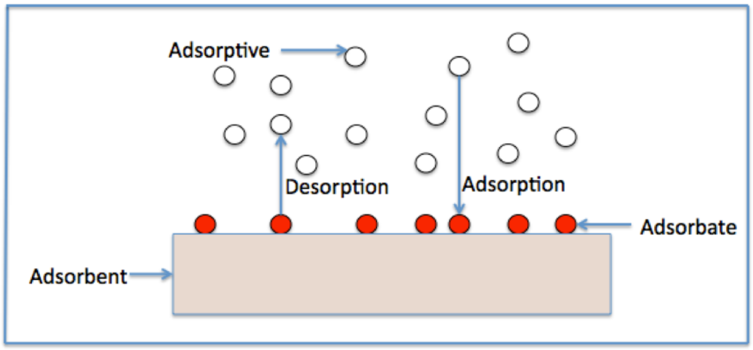

Figure 1.1: Schematic representation of adsorption

1.2 Selective Adsorption

Gas separation by adsorption can be accomplished by three basic physical mechanisms: equilibria, kinetics and steric effects. Equilibria mechanisms rely on the strength of the attraction between gas molecules and the substrate, while kinetic mechanisms involve the differences in the adsorption and transport rates of a gas on and through the substrate [5]. Steric mechanisms, on the other hand, depend on the incompatibility between the size or shape of the adsorbate gas molecules and the pores of the substrate. For instance, since CO_2 is typically found in a mixture with gases of similar size (such as CH_4 and H_2), but different shape, steric separation may be effective. Also, CO_2 is usually subjected to the strongest, attractive interactions with substrates; for example, in this study we found that the energy of interaction of CO_2 with graphite is 35% stronger than CH_4 with graphite. As a result, the equilibrium mechanism may also present an effective strategy.

Adsorption selectivity in a binary mixture of components i and j is defined as

$$S(i/j) = \frac{x_i/x_j}{y_i/y_j}, \tag{1.1}$$

where x_i and y_i are the molar concentration in the adsorbed phase and the initial molar concentration in the vapor phase of species i, respectively. The concentration in the adsorbed phase, x_i, can be obtained from molecular dynamics simulation.

1.3 Health and Environmental Issues

As a result of human activity, approximately 7 GT of carbon is emitted in the earth's atmosphere each year [22]. According to the report in Ref [23], the global average atmospheric carbon dioxide in 2017 was 405.0 ppm. Deforestation, burning oil and coal, industrial processes, and transportation emissions are the primary causes of increased carbon dioxide concentrations in the atmosphere [22]. CO_2 removal is important for air purification and environmentally significant for the minimization of its effect on global warming [3, 9].

To reduce the atmospheric level of CO_2, effective strategies have been proposed: separation and sequestration of CO_2, better fuel efficiency in power production and transportation, and using alternate power sources such as, nuclear, solar, and wind energy [4, 22].

Nitrogen dioxide is one of the major toxic gases contributing to air pollution. NO_2 is primarily released in the air from burning fuel. Sources of NO_2 are emissions from cars, trucks and buses, power plants, and off-road equipment [1]. Gasana et al. reported that exposure to nitrogen dioxide is positively associated with a higher incidence of childhood asthma [24]. Experimental evidence from Ref [25] illustrates that there is a high rate of lung damage in laboratory animals after being exposed to this detrimental gas. Due to these adverse effects on the human respiratory system, there is currently an urgent need to restrict the concentration of NO_2 in the atmosphere.

Chapter 2

Methodology

In this chapter, we describe the models of the molecules and substrates that we use in this study and the interactions between the molecules and the molecule-substrate. We also explain the simulation method.

2.1 Molecular Models

2.1.1 N_2

Nitrogen is a diatomic molecule which represents 78.08% of the composition of air. It is an inert gas at standard temperature and pressure, nonmetallic, colorless and odorless. It has a mass of 28 g/mol, density of 1.25 g/l, and triple point temperature of 63.18 K [26]. It has zero electric dipole moment, while its electric quadrupole moment is 1.52×10^{-26} esu cm^2, which is less than half of the quadrupole moment of CO_2 [27].

In our simulations, the N_2-N_2 intermolecular interaction is represented by a Lennard Jones (LJ) potential, with one LJ site located at the center. The LJ potential is given by,

$$U_{LJ} = 4\epsilon\left[\left(\frac{\sigma}{r}\right)^{12} - \left(\frac{\sigma}{r}\right)^{6}\right], \tag{2.1}$$

where ϵ and σ are the energy and size LJ parameters, respectively, and r is the distance between atoms. The first term in equation (2.1) represents the electronic repulsive force and the second term represents the van der Waals attractive force. The LJ parameters for N_2 were obtained from ref [28], $\epsilon = 95.05$ K and $\sigma = 3.698$ Å.

2.1.2 CH_4

Methane is the main constituent of natural gas fuel. It is a gas at 298 K, and 1 atm, its mass is 16 g/mol, and its density is 0.656 g/l. Methane has critical and triple point temperatures of 190.56 K and 90.69 K, respectively. We represent CH_4 as a neutral spherical molecule with zero electric dipole and quadrupole moments [27].

The CH_4-CH_4 intermolecular interaction is modeled as a LJ potential with one site, given by equation (2.1). The LJ parameters are ϵ= 148.0 K and σ= 3.7 Å [4].

2.1.3 CO_2

CO_2 is a colorless odorless gas at standard temperature and pressure. The dipole moment of CO_2 is zero, and the electric quadrupole moment is Q= 4.30×10^{-26} esu cm^2 [27]. Its mass, density, and triple point are equal to 44 g/mol, 1.96 g/l, and 216.55 K, respectively. We describe the CO_2 molecule as a linear rigid body with three LJ sites and three partial charges placed on each atom. The carbon atom has a positive charge $q_C = 0.576e$ and the oxygen atoms have a negative charge $q_O = -0.288e$. The bond length is b=1.18 Å and the bond angle is $\theta = 180°$, as it appears in Figure 2.1 [4].

The CO_2-CO_2 intermolecular interactions are modeled by a combination of the LJ and Coulomb potentials between partial charges as shown in equation (2.2),

$$U(\vec{r}) = \sum_{ij} \left\{ 4\epsilon_{ij} \left[\left(\frac{\sigma_{ij}}{r_{ij}} \right)^{12} - \left(\frac{\sigma_{ij}}{r_{ij}} \right)^{6} \right] + k_e \frac{q_i q_j}{r_{ij}} \right\} \tag{2.2}$$

where the pairwise summation is over atoms i and j in each respective molecule. The Coulombic part accounts for the interaction between the partial charges. We obtained the LJ parameters from Ref [4] (see Table 2.1).

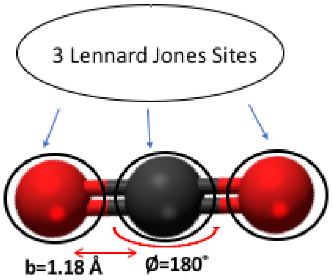

Figure 2.1: Model of the CO_2 molecule

Table 2.1: Lennard Jones and Coulombic Potential Parameters

Adsorbate	ϵ(K)	σ(Å)	$q(e)$
CH_4	148.0	3.7	0
C in CO_2	29.7	2.8	+0.576
O in CO_2	83.0	3.0	-0.288
C in Graphene	28	3.4	0

For different species, the cross parameters are calculated by using the Lorentz-Bertholet combination rules [14],

$$\sigma_{ij} = \frac{\sigma_{ii} + \sigma_{jj}}{2} \tag{2.3}$$

$$\epsilon_{ij} = \sqrt{\epsilon_{ii}\epsilon_{jj}} \tag{2.4}$$

2.1.4 NO_2

Nitrogen dioxide is a reddish-brown gas above 294.3 K, with a pungent, acrid odor, it becomes a yellowish-brown liquid below 294.3 K, and converts to the colorless dinitrogen tetroxide, N_2O_4, below 261.9 K and 1 atm. The NO_2 molecule is a polar molecule with a dipole moment of $P = 0.316 \times 10^{-18}$

(esu cm) [27]. The mass, density, triple point and critical temperatures are 46 g/mol, 2.05 g/l, 261.95 K, and 431K, respectively.

We model the NO_2 - NO_2 intermolecular interaction by the TIP3P potential which stands for three-site transferable intermolecular potential with only one LJ site and three partial charges [29]. The nitrogen atom has a positive charge $q_N = 0.28e$ and the oxygen atoms have negative charges $q_O = -0.14e$. The model of NO_2 is shown in Figure 2.2. The bond length is b=1.193 Å and the bond angle is $\theta = 134.1°$ [30].

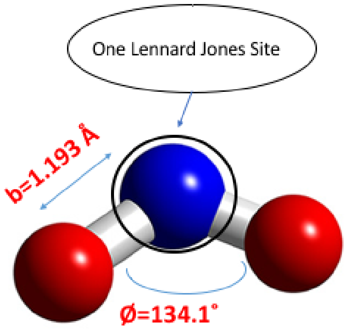

Figure 2.2: Model of the NO_2 molecule

The NO_2 - NO_2 interaction is a combination of the LJ and Coulomb potentials given by equation (2.2). The LJ interaction site is located at the nitrogen atom, and the LJ parameters are adopted from Ref. [31], $\epsilon = 210$ K and $\sigma = 3.765$ Å.

The NO_2 molecule is assumed non-rigid, with bond and angle elastic energies as shown in the following equations,

$$U_b = \frac{1}{2}k_1\left(\delta l_1^2 + \delta l_2^2\right), \tag{2.5}$$

$$U_a = \frac{1}{2}k_2 l^2(\delta\alpha)^2, \tag{2.6}$$

where k_1 and k_2 are the elastic constants for the bond stretch and the angle bend, respectively. δl_i is the displacement from the equilibrium of bond i, l is the equilibrium bond length and $\delta\alpha$ is the displacement from the equilibrium of the angle α. In order to evaluate these energies, we calculate k_1 and k_2 from spectroscopic data of the frequencies of the normal modes.

We obtain the vibrational modes of the triatomic molecule by the method of small oscillations. The Lagrangian of the molecule represented in Figure 2.3 is [32],

$$L = \frac{1}{2}m_A\left(\dot{u}_1^2 + \dot{u}_3^2\right) + \frac{1}{2}m_B\dot{u}_2^2 - \frac{1}{2}k_1\left(\delta l_1^2 + \delta l_2^2\right) - \frac{1}{2}k_2 l_0^2(\delta\alpha)^2, \tag{2.7}$$

where u_i is the displacement of the atom i, l_1 is the distance between atoms 1 and 2, l_2 is the distance between atoms 2 and 3, α is half the angle ABA, l_0 is the equilibrium bond length, m_A and m_B are the masses of O and N respectively, and k_1 and k_2 are the elastic constants of the bond stretch and angle bend, respectively. The frequencies of the normal modes satisfy the relation,

$$\omega^4 - \omega^2\Big[\frac{k_1}{m_A}\left(1 + \frac{2m_A}{m_B}\cos\alpha^2\right) + \frac{2k_2}{m_A}\left(1 + \frac{2m_A}{m_B}\sin\alpha^2\right)\Big] + \frac{2\mu k_1 k_2}{m_A^2 m_B} = 0, \tag{2.8}$$

where μ is the total mass and α is the equilibrium angle. The frequencies of the normal modes from spectroscopy data [33], are $\omega_1 = 1318.0$ cm^{-1} and $\omega_2 = 750.0$ cm^{-1} for the symmetric stretch and symmetric bending, respectively. These two modes are shown in Figure 2.4. By inserting ω_1 and ω_2 in equation (2.8), we obtain the values of the elastic constants k_1 and k_2 equal to 772.466 kcal/(mol Å^2) and 123.720 kcal/(mol rad^2), respectively.

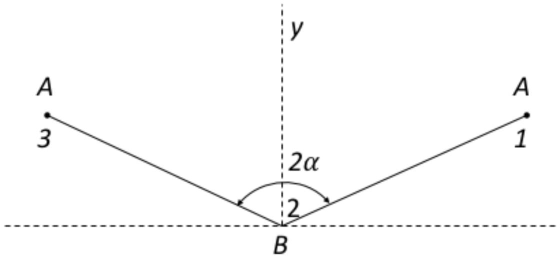

Figure 2.3: Triangular molecule NO_2 where A is the Oxygen atom and B is the Nitrogen atom.

(a) symmetric stretch

(b) symmetric bending

Figure 2.4: Vibrational modes of triangular molecule NO_2 considering symmetric stretch and symmetric bending.

2.2 Substrates

2.2.1 Graphite

Graphite is a form of carbon made up of stacked layers of graphene. In each layer, the carbon atoms are arranged in a honeycomb lattice with separation 1.42 Å, and the distance between planes is 3.4 Å. Atoms in the plane are bonded covalently while bonding between layers is via Van der

Waals forces, which allow layers of graphite to be easily separated, as shown in Figure 2.5.

In our simulation, we treat graphite as continuous matter. The continuous approximation calculates the interaction between an atom and the entire slab of graphite instead of doing the sum over all carbon atoms.

The interaction between an adsorbate atom and the graphite substrate is described as the Steel-1043 potential [34] given by,

$$U_{Steel}(z) = 2\pi\epsilon\rho\sigma^2\Delta\left[\frac{2}{5}\left(\frac{\sigma}{z}\right)^{10} - \left(\frac{\sigma}{z}\right)^{4} - \left(\frac{\sigma^4}{3\Delta\left(z+0.61\Delta\right)^3}\right)\right], \qquad (2.9)$$

where ϵ and σ are the LJ parameters, z is the distance between the adatom and the graphite surface; the number of carbon atoms per unit volume in graphite is $\rho = 0.114$ Å^{-3}, and the separation distance between the layers of graphitic carbon is $\Delta = 3.35$ Å .

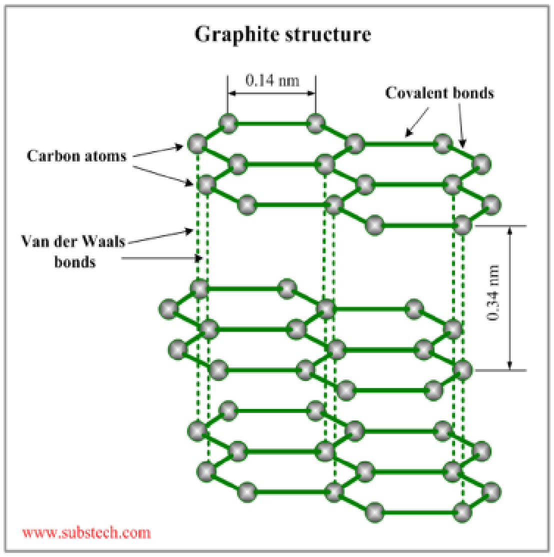

Figure 2.5: Graphite

2.2.2 Graphene and Graphene Nanoribbons

Graphene nanoribbons (GNRs) are quasi one dimensional carbon structures that can be obtained by “cutting a graphene sheet into strips of nanometer width [35]. Graphene is a unique material with high specific surface area of ~2600 m^2/g, which is obtained from graphite through oxidation, exfoliation, and reduction [13]. In 2010, Andre Geim and Konstantin Novoselov were awarded the Nobel Prize in physics for fabricating high quality graphene crystallites using "scotch-tape" method [36]. Graphene is a promising material for many applications in nano-electronics, energy storage, biosensing, conductivity, structure stability, and charge transport ability [37–40]. The carbon atoms in graphene are arranged in a hexagonal honeycomb lattice. Ever since the experimental isolation of graphene in 2004, significant research effort has been focused on investigating the electronic and transport properties of its nanoribbons. A number of techniques have been developed in order to fabricate GNRs. These include electron beam lithography and etching, chemical synthesis and unzipping of carbon nanotubes [41]. The properties of graphene nanoribbons can be tuned from metallic to semiconducting through by the widths and the edge styles [42]. We use GNRs in our simulations as a filter to select molecules. GNRs are effective because the gap opening can be adjust to control the selectivity.

2.3 Interaction Between Molecules and Substrates

2.3.1 CO_2/CH_4-Graphite

As mentioned in section 2.2.2, the model of the interaction between a semi-infinite pore wall of graphite and an adsorbate site is described as the Steel-1043 potential as shown in equation (2.10),

$$U_{Steel}(z) = 2\pi\epsilon\rho\sigma^2\Delta\left[\frac{2}{5}\left(\frac{\sigma}{z}\right)^{10} - \left(\frac{\sigma}{z}\right)^{4} - \left(\frac{\sigma^4}{3\Delta\left(z+0.61\Delta\right)^3}\right)\right], \tag{2.10}$$

where ϵ and σ are the LJ parameters (adsorbate-C) calculated by using the Lorentz-Bertholet combination rules. The number of carbon atoms per unit volume in graphite is $\rho = 0.114$ Å^{-3}, the separation distance between the layers of graphitic carbon is $\Delta = 3.35$ Å , and z is the distance between the adsorbate and the graphite surface [6]. The parameters used in the simulation are summarized in Table 2.2. Figure 2.6 represents the interaction between graphite and adsorbents CO_2 and CH_4 using the Steel-1043 potential. For CO_2, we show two orientations, vertical (V) and horizontal (H); at the horizontal orientation the interaction with the wall is stronger and more attractive, while for the vertical case it is the least energetically favorable. Also, the interaction between graphite and CO_2 in the horizontal case is stronger than the interaction with CH_4, as seen in Figure 2.6.

Table 2.2: Potential parameters for CH_4-C and CO_2-C interactions.

Adsorbate	ϵ(Kcal/mol)	σ(Å)
CH_4	0.12788	3.55
C in CO_2	0.05728	3.1
O in CO_2	0.09576	3.2

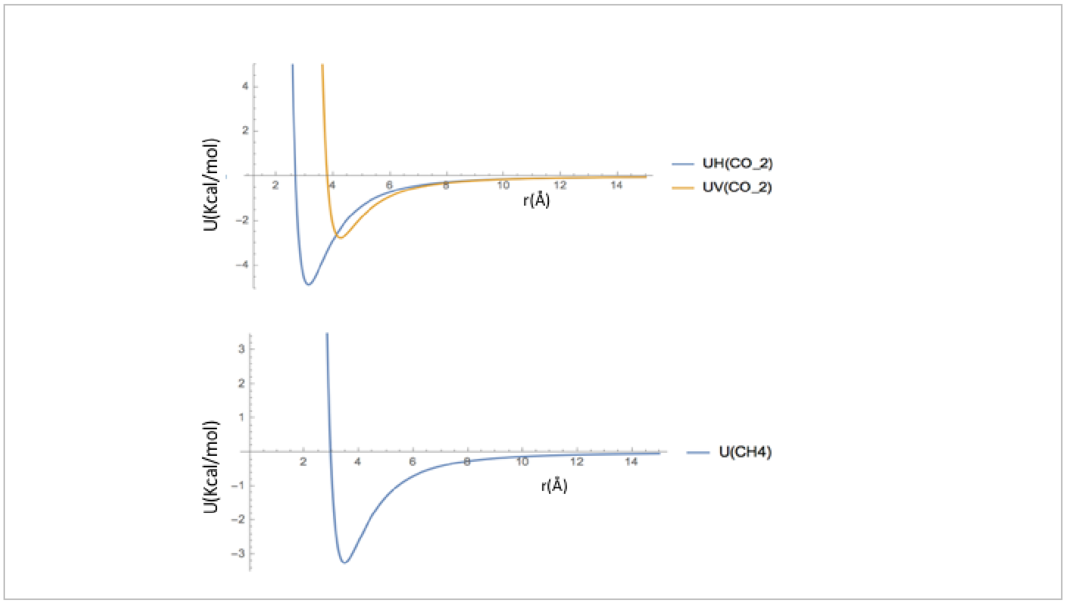

Figure 2.6: Interaction energy between graphite and adsorbates CO_2 and CH_4 using Steel-1043 potential. At the top, CO_2-graphite with two orientations for CO_2: vertical (V) and horizontal (H). At the bottom, we show CH_4-graphite.

2.3.2 CO_2/CH_4-GNRs

We describe the interaction between GNRs and adsorbates by a sum of LJ potentials as shown in equation (2.11),

$$U_{LJ} = \sum_{ij} U_{LJ}^{ij}, \tag{2.11}$$

where i represents the C atoms in GNRs, and j represents the adatom. For cross parameters, we use equations (2.3) and (2.4). The LJ parameters for C are taken from Ref [7], (see Table 2.1). The GNRs are kept rigid and fixed during the simulations.

2.4 Simulation Method

2.4.1 Molecular Dynamics Simulation

Molecular Dynamics (MD) Simulation is a computational method for calculating the equilibrium and transport properties of model classical systems, and is applicable when studying adsorption of different molecules. The simulation is prepared by selecting the model of the system that consists of N particles. Then, the system evolves following Newton's equations of motion until the properties stabilize over time. After that, the quantities of interest are measured. The process of the MD simulation requires the assignment of initial positions and velocities to all particles in the system [44]. The next step is to calculate the force between the particles that are not beyond the cut-off range of the potential. In particular, the x- component of the force is computed by using the following relation,

$$f_x(r) = -\frac{\partial u(r)}{\partial x} = -\left(\frac{x}{r}\right)\left(\frac{\partial u(r)}{\partial r}\right) \tag{2.12}$$

Hence, for the Lennard-Jones potential, the force in reduced units is given by,

$$f_x(r) = \frac{48x}{r^2}\left(\frac{1}{r^{12}} - 0.5\frac{1}{r^6}\right) \tag{2.13}$$

After calculating the forces between the particles, the Newton's equations of motion are integrated using the Verlet algorithm given by the following equation

$$r(t+\Delta t) \approx 2r(t) - r(t-\Delta t) + \frac{f(t)}{m}\Delta t^2, \tag{2.14}$$

where Δt is the chosen time step in the MD simulation. Since the Verlet algorithm does not use the velocity to compute the new position, the velocity can be derived from the knowledge of the trajectory using the following expression,

$$v(t) = \frac{r(t + \Delta t) - r(t - \Delta t)}{2\Delta t} + O(\Delta t^2), \tag{2.15}$$

The basic MD technique computes the natural time evolution of a classical system with N particles in a volume V in the microcanonical ensemble (NVE) where the energy is constant. Simulations in the canonical ensemble (NVT) where the temperature is constant can also be performed. There are two ways to operate such simulations. The first one is a mixture of Newtonian MD with some Monte Carlo moves. The second one is a modified form of the Lagrangian equations of motion, usually called the extended Lagrangian method [44]. In this work we run NVT-MD simulations by using the Nose-Hoover thermostat, which is based on the extended Lagrangian method. The Lagrangian is given by,

$$\mathcal{L}_{Nose} = \sum_{i=1}^{N} \frac{m_i}{2} s^2 \dot{r}_i^2 - \mathcal{U}(r^N) + \frac{Q}{2}\dot{s}^2 - \frac{L}{\beta}\ln s, \tag{2.16}$$

where L is a parameter and Q is an effective mass associated with the artificially introduced coordinate s. The Nose-Hoover Hamiltonian is given by,

$$\mathcal{H}_{Nose} = \sum_{i=1}^{N} \frac{p_i^2}{2m_i s^2} + \mathcal{U}(r^N) + \frac{p_s^2}{2Q} + L\frac{\ln s}{\beta}, \tag{2.17}$$

where $p_i \equiv \frac{\partial \mathcal{L}}{\partial \dot{r}_i} = m_i s^2 \dot{r}_i$, and $p_s \equiv \frac{\partial \mathcal{L}}{\partial \dot{s}} = Q\dot{s}$.

The temperature in the MD simulation is obtained from the average kinetic energy (KE),

$$\frac{3}{2}k_B T = \langle KE \rangle, \tag{2.18}$$

where k_B is the Boltzmann constant. The pressure is obtained by using the virial equation,

$$P = \rho\, k_B T + \frac{1}{dV}\langle \sum_{i<j} f(\vec{r_{ij}}).\vec{r_{ij}} \rangle, \tag{2.19}$$

where ρ is the density, V is the system volume, d is the dimensionality of the system, and $f(r_{ij})$ is the force between particles i and j at a distance r_{ij}.

We run our simulations with the LAMMPS program, which stands for (Large-scale Atomic/ Molecular Massively Parallel Simulator) [45]. LAMMPS is a molecular dynamics simulation code designed to run efficiently on parallel computers, and it models an ensemble of particles in a liquid, solid, or gaseous state. Also, it can model atomic, polymeric, biological, metallic, granular, and coarse-grained systems using a variety of force fields and boundary conditions [46].

The first system that we simulate is the binary mixture of NO_2/N_2 on gold. We begin the simulation by creating a cubic box of dimensions 80 Å in X,Y,and Z. We locate the gold substrate at the bottom of the box as in Figure 2.7. The gold slab is 8.16 Å tall. We set the boundary conditions to be periodic in XY whereas reflective in Z directions. Next, we deposit the molecules (NO_2 and N_2) inside the box with the forces of the gold turned-off, and run NVT until the system equilibrates. Then we turn the forces of the gold on and run NVT again for 6 million fs-timesteps. We repeat the simulations using temperatures in the range 200 K to 400 K. For each temperature, we use various densities. We obtain the number of adsorbed molecules by counting the number that are located in a region of height 5 Å above the gold substrate.

The second system that we study is the CO_2/CH_4 binary mixture on graphene nanoribbons (GNRs) suspended on graphite. We set the simulation box with 160 Å side lengths, periodic boundaries in XY directions, while the Z direction is a reflective wall. We put the GNRs above the graphite substrate at an adjustable distance from 6 Å through 14 Å increasing by 2 Å increments. We control the gap separation between GNRs by using several openings, as shown in the simulation box in Figure 2.8. The positions of the graphene's carbon atoms, which remain fixed during the simulations, are calculated by a FORTRAN code and then read by the LAMMPS program (see appendix A and B for more details).

The nanoribbons are created by cutting the graphene sheet at variable gap separations, so that the carbon atoms within that region are deleted. By cutting the graphene layer in the Y direction, we obtain zigzag graphene nanoribbons (ZGNRs), whereas cutting the graphene layer in the X direction, gives armchair graphene nanoribbons (AGNRs). By manipulating the region where the carbon atoms are deleted, we get two different styles of edges, as shown in Figure 2.9.

Figure 2.9 represents the ZGNRs in the upper row and AGNRs in the lower row with two different styles: VV or VB. In style VV the vertexes are facing vertexes and the beds are facing beds. For style VV the separations are given in terms of parameters b and c for ZGNRs and parameters e and f for AGNRs, which are the distance from bed to bed and vertex to vertex, respectively. In style VB where the vertexes are facing the beds, the distances between them are given by parameters a and d in ZGNRs and AGNRs respectively. In the simulations, we first deposit 50 CO_2 molecules and 50 CH_4 molecules with the substrate's forces turned off and run the NVT at 300 K until the system equilibrates. Then we open the slit of GNRs, turn the forces on, and run NVT again for 6 million fs- timesteps. The molecules are attracted to the graphene, and pass through the slit. The molecules that enter through the slit form layers on the graphite surface and on the bottom of the GNRs.

For both systems studied (NO_2/N_2 on gold and CO_2/CH_4 on GNRs-graphite), we calculated the selectivity and the rate of adsorption. The results are presented in chapter 3.

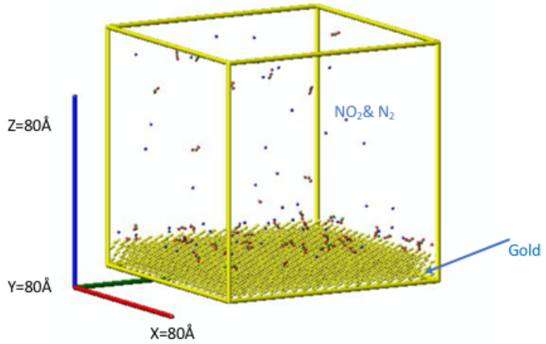

Figure 2.7: Simulation box for the NO_2/N_2 binary mixture with the gold substrate at the bottom.

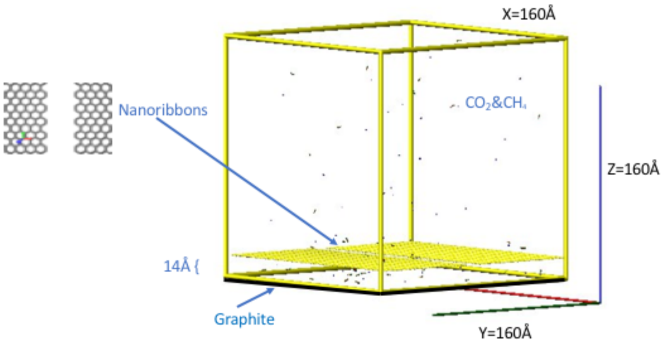

Figure 2.8: Simulation box for CO_2/CH_4 binary mixture with the GNRs and graphite at the bottom.

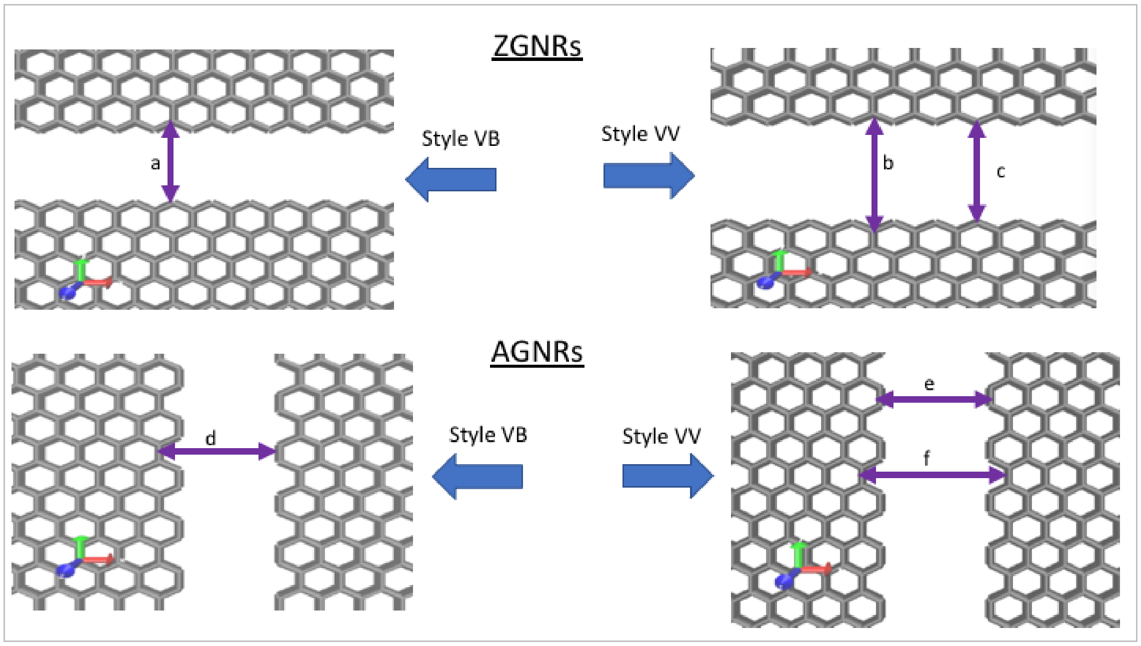

Figure 2.9: In the upper row, ZGNRs with two styles; in the left, style VB with parameter a and in the right, style VV with parameters b and c. In the lower row, AGNRs with two styles; in the left, style VB with parameter d and in the right, style VV with parameters e and f.

2.4.2 Boundary Conditions

During the MD simulation, the particles may move out of the box. By setting periodic boundary conditions in the XY directions, whenever the particle moves out of the box, it re-enters from the adjacent replica with the same speed, as shown in Figure 2.10. In the Z direction, the boundary condition is reflective, so that any molecule that hits the boundary will be reflected back. In the simulations of the mixture of molecules with a substrate, we set the boundary condition to be periodic in X and Y, while reflective in the Z direction. In this way, we represent an infinite system in X and Y directions. For the simulations without a substrate, we set the boundary to be periodic in X Y Z, corresponding to an infinite 3D-bulk system.

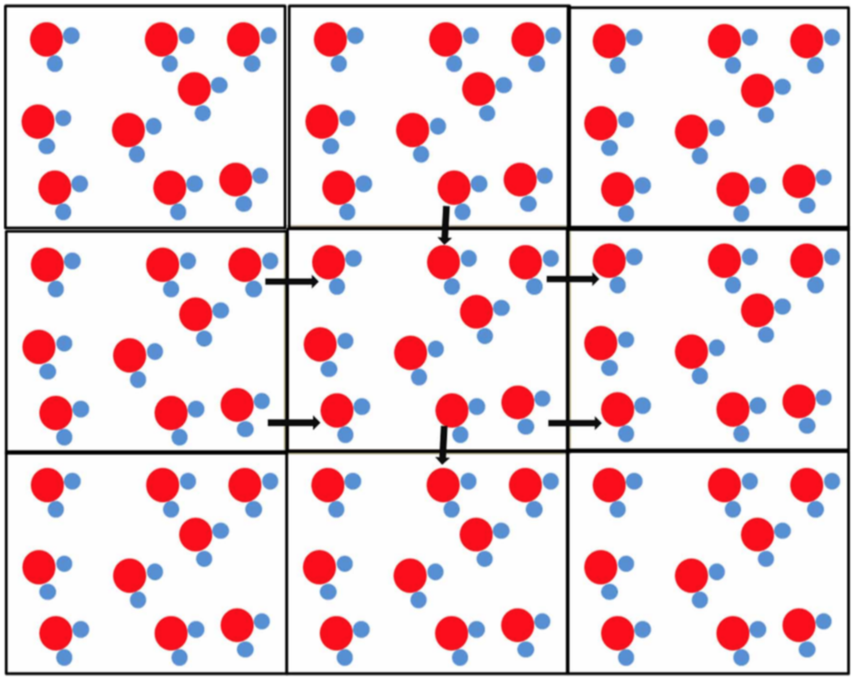

Figure 2.10: Representation of periodic boundary condition

Chapter 3

Equilibrium Physical Properties of Pure Vapors

We run MD simulations for the N_2, CO_2 and CH_4 vapors individually to confirm that our models reproduce the experimental values of pressure at 1 atm, for temperatures from 200 K to 500 K. We set periodic boundary conditions in all directions of the cubic box. We insert specific numbers of molecules in the simulation box for each given density. In the MD simulations, the pressure is calculated using equation (2.19). The equilibrium pressure was determined by running the simulation for 5 to 10 million time-steps and averaging the last two million values. Ultimately, we compare the average equilibrium pressure obtained in the simulation with the experimental value.

3.0.1 N_2

N_2 molecules were added to a cubic simulation box with a side length of 120 Å , as shown in Figure 3.1. We set the density and temperature according to the experimental values [26]. As it appears in Table (3.1), the MD pressures are less than 5% from the experimental value. In summary, we confirm that the interaction potential used for N_2 is reliable.

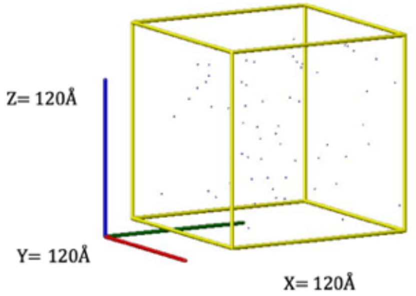

Figure 3.1: Simulation box for bulk N_2.

Table 3.1: Test of the simulation pressure vs. experimental pressure for N_2.

Temperature (K)	Density (mol/L)	Exp.Pressure (atm)	MD Pressure(atm)	Δ P(%)
200	0.060	0.9869	0.9601	2.7
300	0.040	0.9869	0.9696	1.8
400	0.030	0.9869	0.9403	4.7
500	0.024	0.9869	0.9527	3.5

3.0.2 CO_2

We deposit 111 CO_2 molecules in a simulation box of volume $(160)^3$Å^3 and run the MD simulation at 273 K. The density 0.271×10^{-4}Å^{-3} corresponds to the value 1.978 g/L at STP [47]. The pressure calculated in the MD simulation was 1.02 atm with 2% difference from the real gas.

3.0.3 CH_4

We deposit 101 CH_4 molecules in a simulation box of volume $(160)^3$Å^3 and run the MD simulation at 298 K. The density 0.246×10^{-4}Å^{-3} corresponds to the value 0.656 g/L at STP [48]. The simulation pressure is 0.98 atm with a 2% difference compared with the experimental result (1atm). The small error percentage is an indication of our success in presenting CH_4 as a spherical molecule.

Chapter 4

Adsorption and Selectivity of a Mixture of CO_2 and CH_4 on Graphite

4.1 Approach

Modeling the interaction between an adsorbate and a substrate, is an essential part of the simulation technique. We described the interaction between graphite and the adsorbates in section 2.3.2.

We compute the force between CO_2-CO_2 as a combination of LJ and Coulomb potentials as mentioned in equation (2.2), and the interaction between CH_4-CH_4 as a LJ potential as shown in equation (2.1).

We run MD simulations in the NVT ensemble to compute the adsorption of the binary mixture CO_2/CH_4 on graphite. The simulation cell has a 160 Å length in X Y Z, and the boundary conditions are periodic in XY and reflective in the Z direction, as described in section (2.4).

We run the simulations at room temperature (300K). For each simulation, we collect the average number of molecules in the film on graphite. We plot the fraction of molecules adsorbed as a function of time and we calculate the selectivity given by,

$$S(CO_2) = \frac{x_{CO_2}/x_{CH_4}}{y_{CO_2}/y_{CH_4}}, \tag{4.1}$$

where x_{CO_2} and x_{CH_4} are the concentration in the film on graphite of CO_2 and CH_4 respectively, and y_{CO_2} and y_{CH_4} are the initial concentrations in the vapor of CO_2 and CH_4, respectively.

We define the relative rate of adsorption ,R, as,

$$R = \frac{r_{CO_2}}{r_{CH_4}}, \tag{4.2}$$

where r$_{CO_2}$ and r$_{CH_4}$ are the initial rate of growth adsorption (in molecules/ns) for CO_2 and CH_4 respectively.

4.2 Adsorption on Graphite

We simulate the adsorption of CO_2/CH_4 on graphite at room temperature, and calculate the selectivity and the relative rate of adsorption for CO_2 over CH_4. The results are displayed in Figure 3.2.

In part a), we plot the fraction of CO_2 and CH_4 adsorbed on graphite versus time. We calculate the selectivity by taking the average at equilibrium, which is 1.68. Also, we calculate the relative rate of adsorption, which is 1.88. The adsorption for CO_2 starts at a higher rate than CH_4 as a result of the stronger Van der Waals interaction between CO_2 and graphite.

In part b), we plot the adsorption energy per particle for CO_2 and CH_4 versus time. We see that as molecules adsorb, the adsorption energy per particle rapidly increases in absolute value and remains constant at later times, indicating monolayer adsorption. We found that the adsorption energy for CO_2 is 3.76 Kcal/mol, while for CH_4 is 2.64 Kcal/mol, meaning that the adsorption energy for CO_2 is higher than CH_4 by 42% due to stronger Van der Waals interaction between CO_2 and graphite. These energies are consistent with the minimum potential for the interaction between CO_2-graphite, which is higher than the minimum potential for CH_4-graphite, as seen in Figure 2.6. The V$_{min}$ of CO_2 is 4.8 Kcal/mol, while V$_{min}$ of CH_4 is 3.2 Kcal/mol.

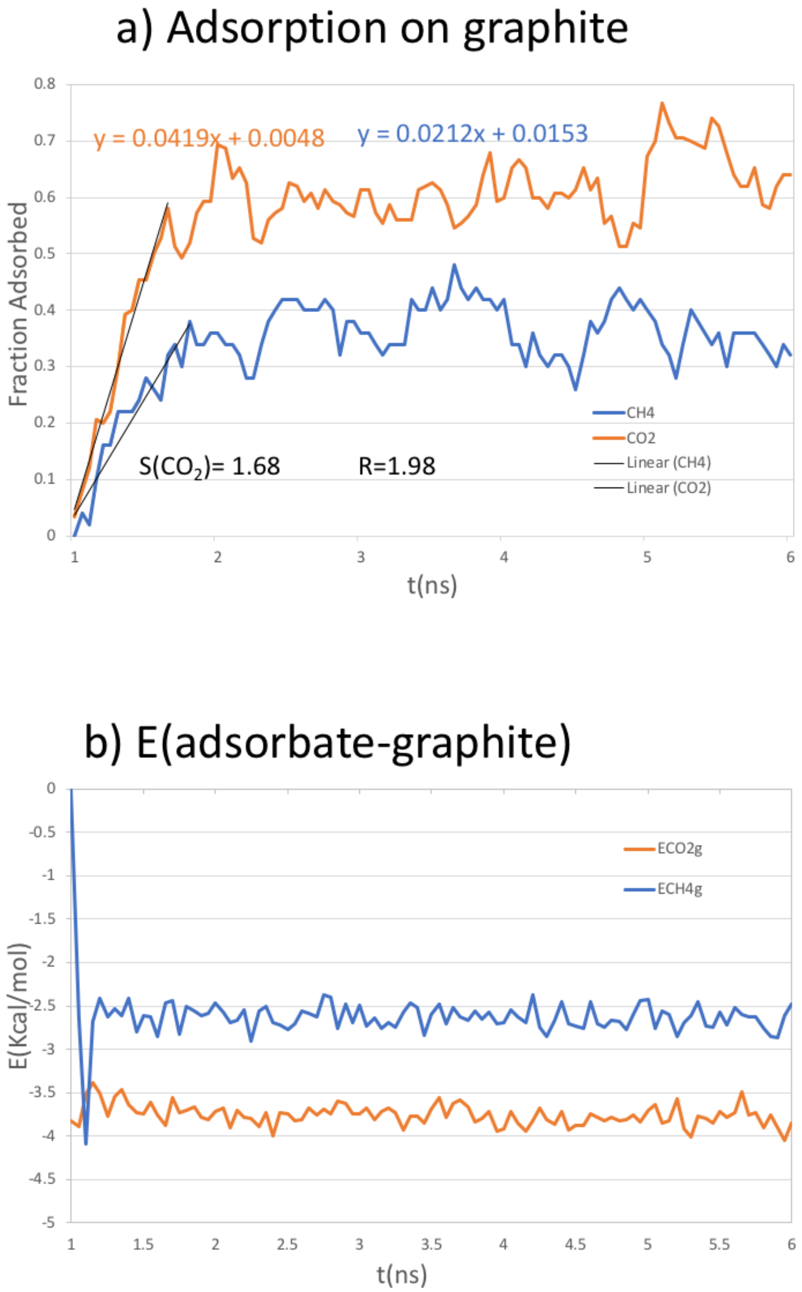

Figure 4.1: a) Adsorption of a binary mixture of CO_2 and CH_4 on graphite vs time(ns). The orange and blue lines indicate the fraction adsorbed on graphite for CO_2 and CH_4 respectively. The equations represent the linear fit for time 1-2 ns, for CO_2 (left) and CH_4 (right). The values of the selectivity and relative rate of adsorption are shown in the insert. b) Interaction energy per particle between graphite and adsorbates; the orange line represents CO_2, and the blue line represents CH_4

References

[1] Report of United States Environmental Protection Agency. Hazardous air pollutants. `https://www.epa.gov/haps`, 2018.

[2] E. Sher. *Handbook of air pollution from internal combustion engines: pollutant formation and control.* Academic Press, 1998.

[3] l. Bastin, P. S. Barcia, E. J. Hurtado, J. A. C. Silva, A. E. Rodrigues, and B. Chen. A microporous metalorganic framework for separation of CO_2/N_2 and CO_2/CH_4 by fixed-bed adsorption. *The J. of Phys. Chem. C*, 112:1575–1581, 2008.

[4] R. Babarao, Z. Hu, and J. Jiang. Storage and separation of CO_2 and CH_4 in silicalite, C_{168} schwarzite, and IRMOF-1: a comparative study from monte carlo simulation. *Langmuir*, 23:659–666, 2007.

[5] S. M. Gatica, A. Nekhai, and A. Scrivener. Adsorption and gas separation of molecules by carbon nanohorns. *Molecules*, 21, 2016.

[6] M. Heuchel, G. M. Davies, E. Buss, and N. A. Seaton. Adsorption of carbon dioxide and methane and their mixtures on an activated carbon:simulation and experiment. *Langmuir*, 15:8695–8705, 1999.

[7] Y. Liu and J. Wilcox. Molecular simulation studies of CO_2 adsorption by carbon model compounds for carbon capture and sequestration applications. *Environmental Science and Technology*, 47:95–101, 2013.

[8] S. M. Maiga. Adsorption of gases on graphene and metal organic frameworks. *PhD. Dissertation, Howard University Washington, D.C*, 2016.

[9] S. M. Maiga, M. A. Medina, O. J. Durodola, and S. M. Gatica. Simulations of adsorption of CO_2 and CH_4 in MOFs: Effect of the size andcharge distribution on the selectivity. *J. of Low Temperature Phys.*, 172:274–288, 2013.

[10] J. C. Palmer, J. D. Moore, T. J. Roussel, J. K. Brennan, and K. E. Gubbins. Adsorptive behavior of CO_2, CH_4 and their mixtures in carbon nanospace: a molecular simulation study. *Phys. Chem. Chem. Phys*, 13:3985–3996, 2011.

[11] X. Peng, D. Cao, and J. Zhao. Grand canonical monte carlo simulation of methane-carbon dioxide mixtures on ordered mesoporous carbon CMK-1. *Separation and Purification Technology*, 68:50–60, 2009.

[12] L. Lu, D. Nicholson, and S. Bhatia. Adsorption of CH_4 and CH_4/CO_2 mixtures in carbon nanotubes and disordered carbons: A molecular simulation study. *Chem. Engineering Science*, 121:268–278, 2015.

[13] S. Gadipelli and Z. Xiao Guo. Graphene-based materials: Synthesis and gas sorption, storage and separation. *Progress in Materials Science*, 69:1–60, 2014.

[14] L. W. Bruch, M. W. Cole, and E. Zaremba. *Physical Adsorption: Forces and Phenomena.* Clarendon Press, Oxford, 1997.

[15] J. Dai, J. Yuan, and P Giannozzi. Gas adsorption on graphene doped with B, N, Al, and S: A theoretical study. *Applied Phys. Letters*, 95:232105, 2009.

[16] I. Choudhuri, N. Patra, A. Mahata, R. Ahuja, and B. Pathak. B-N@graphene: Highly sensitive and selective gas sensor. *J. of Phys. Chem. C*, 119:24827–24836, 2015.

[17] T. O. Wehling, K. S. Novoselov, S. V. Morozov, E. E. Vdovin, M. I. Katsnelson, A. K. Grim, and A. I. Lichtenstein. Molecular doping of graphene. *Nano Letter*, 8:173–177, 2008.

[18] E. S. Alldredge, S. C. Badescu, N. Bajwa, F. K. Perkins, E. S Snow, and T. L. Reinecke. Adsorption of nitro-substituted aromatics on single-walled carbon nanotubes. *Phys. Rev. B*, 82:125418, 2010.

[19] D. T. Wickham, B. A. Banse, and B. E. Koel. Adsorption of nitrogen dioxide on polycrystalline gold. *Catalysis Letters*, 6:163–172, 1990.

[20] W. Yim, X.G. Gong, and Z. Liu. Chemisorption of NO_2 on carbon nanotubes. *The J. of Phys. Chem. B*, 107:9363–9369, 2003.

[21] D. Leenaerts, B. Partoens, and F. Peeters. Adsorption of H_2O, NH_3, CO, NO_2, and NO on graphene: A first-principles study. *Phys. Rev. B*, 77:125416, 2008.

[22] D. Aaron and C. Tsouris. Separation of CO_2 from flue gas: A review. *Separation Science and Technology*, 40:321–348, 2005.

[23] R . Lindsey. Climate change: Atmospheric carbon dioxide. `https://www.climate.gov/news-features/understanding-climate/climate-change-atmospheric-carbon-dioxide`, 2018.

[24] J. Gasana, D. Dillikar, A. Mendy, E. Forno, and V. E. Ramos. Motor vehicle air pollution and asthma in children: A meta-analysis. *Environmental Research*, 117:36–45, 2012.

[25] D. E. Azoulay, M. Torres, P. Soler, and J. Moreau. Pulmonary NO_2 toxicity in neonate and adult guinea pigs and rats. *Environmental Research*, 30:322 – 339, 1983.

[26] R. L. David. *CRC Handbook of Chemistry and Physics*. CRC Press, 88th edition, 2007.

[27] J.-R. Li, R.J. Kuppler, and H. C. Zhou. Selective gas adsorption and separation in metalorganic frameworks. *Chem. Soc. Rev*, 2009.

[28] S. M. Gatica, M. K. Kostov, and M. W. Cole. Ordering transition of gases adsorbed on a C_{60} surface: Monte carlo simulations and lattice-gas models. *Phys. Rev. B*, 78, 2008.

[29] W.L. Jorgensen, J. Chandrasekhar, and J. D. Madura. Comparison of simple potential functions for simulating liquid water. *The J. of Chem. Phys.*, 79:926–935, 1983.

[30] G. Murdachaew, M. E. Varner, L. F. Phillips, B. J. Finlayson-Pitts, and R. B. Gerber. Nitrogen dioxide at the air–water interface: trapping, absorption, and solvation in the bulk and at the surface. *Phys. Chem. Chem. Phys.*, 15:204–212, 2013.

[31] R. A. Svebla and R. S. Brokaw. Thermodynamic and transport properties for the N_2O_4 yields $2NO_2$ yields $2NO+O_2$ (reversible reaction) system. *NASA Technical Note*, D, 1966.

[32] L. D. Landau and E. M. Lifshitz. *Mechanics: Course of Theoretical Physics*, volume 1. Elsevier, third edition, 1976.

[33] National Institute of Standards and Technology. NO_2^{14}. `http://webbook.nist.gov/cgi/formula?ID=B4000062&Mask=800`, 2016.

[34] William A. Steele. The physical interaction of gases with crystalline solids: I. gas-solid energies and properties of isolated adsorbed atoms. *Surface Science*, 36:317–352, 04 1973.

[35] V. A. Soroko, K. G. Batrakov, and L. A. Chrnozatonskii. Edge-modified zigzag-shaped graphene nanoribbons: Structure and electronic properties. *Phys. of the Solid State*, 56:2135–2145, 2014.

[36] A. Geim and K. Novoselov. The nobel prize in physics. `https://www.nobelprize.org/prizes/physics/2010/press-release/`, 2010.

[37] J. Kysilka, M. Rubes, L. Grajciar, P. Nachtigall, and O. Bludsky. Accurate description of argon and water adsorption on surface of graphene-based carbon allotropes. *The J. of Phys. Chem. A*, 115:11387–11393, 2011.

[38] X. Zhao. A simple function for calculating the interaction between a molecule and a graphene sheet. *arXiv:1209.4248 [cond-mat.mes-hall]*, 2012.

[39] A. Gutes, B. Hsia, A. Sussman, W. Mickelson, A. Zettl, C. Carraro, and R. Maboudian. Graphene decoration with metal nanoparticles: Towards easy integration for sensing applications. *Nanoscale*, 4:438–440, 2012.

[40] A. Ambrosetti and P. L. Silvestrelli. Adsorption of rare-gas atoms and water on graphite and graphene by van der waals-corrected density functional theory. *The J. of Phys. Chem. C*, 115:3695–3702, 2011.

[41] A. Orlof, J. Ruseckas, and I. V. Zozoulenko. Effect of zigzag and armchair edges on the electronic transport in single-layer and bilayer graphene nanoribbons with defects. *Phys. Rev. B*, 88:125409, 2013.

[42] W. Yin, Y. Xie, L. Liu, Y. Chen, R. Wang, X. Wei, J. Zhong, and L. Lau. Atomic structure and electronic properties of folded graphene nanoribbons: A first-principles study. *J. of Applied Phys.*, 113:173506, 2013.

[43] E. Cheng, M. W. Cole, W. F. Saam, and J. Treiner. Wetting transitions of classical liquid films: A nearly universal trend. *Phys. Rev. B*, 48:18214–18221, 1993.

[44] D. Frenkel and B. Smit. *Understanding Molecular Simulation: from Algorithms to Applications*, volume 1. Academic press, 2002.

[45] `http://lammps.sandia.gov`.

[46] S. Plimpton. Fast parallel algorithms for short-range molecular dynamics. *J. of Computational Phys.*, 117:1–19, 1995.

[47] National Institute of Standards and Technology. Thermophysical properties of carbon dioxide. `https://webbook.nist.gov/cgi/cbook.cgi?ID=C124389&Units=SI`, 2018.

[48] National Institute of Standards and Technology. Thermophysical properties of methane. `https://webbook.nist.gov/cgi/cbook.cgi?Name=CH4&Units=SI`, 2018.